J. Fluid Mech. (1978), *vol.* 84, *part* 1, *pp.* 33–53
Printed in Great Britain

Velocity measurements in an oscillating plane jet issuing into a moving air stream

By J. M. SIMMONS,

Department of Mechanical Engineering,
University of Queensland, St Lucia, Australia

M. F. PLATZER

Department of Aeronautics, Naval Postgraduate School,
Monterey, California

AND T. C. SMITH

Department of Mechanical Engineering,
University of Queensland, St Lucia, Australia

(Received 25 February 1977 and in revised form 13 June 1977)

Hot-wire anemometer measurements in a plane jet issuing at a harmonically oscillating angle into a moving air stream have been made to aid the understanding of oscillatory jet flows in general and flow past aerofoils with oscillating jet flaps in particular. The rates of velocity decay and jet spreading are shown to be greater and less, respectively, than those for a steady jet parallel to the air stream. The shapes of instantaneous velocity profiles and limited measurements of turbulence intensity are similar to those for a steady jet in a parallel air stream if a correction is made for the small velocity difference across the curved jet. The motion of the jet centre-line indicates that flow path lines are similar to those for a steady jet flap over a significant range of frequency of jet oscillation. Finally, a quasi-steady jet flap theory is proposed for an analytical description of the major flow features.

1. Introduction

The steady jet has been studied in considerable detail over the past few decades because of its obvious engineering importance in a number of fields. Much of the available information on steady jet flows has been summarized recently by Harsha (1971). On the other hand, the unsteady jet has received much less attention although an understanding of its flow characteristics is of both fundamental and applied interest in various fields, such as turbulent transport processes, fluidics, acoustics and aeronautics. Early interest in unsteady jet flow phenomena was generated during the development of the pulse jet engine in the 1930s and 1940s. Since then some effort has been devoted to the investigation and use of unsteady jet flow phenomena for energy transfer and pressure exchange purposes (e.g. the work of Lockwood (1963), Johnson & Yang (1968) and Berner & Hermann (1972) on pulse jet augmentation and of Foa (1958) on wave exchange processes). More recently, the advent of fluidics and the growing need for jet noise control motivated studies such as those by Viets (1975) and Bremhorst & Harch (1977).

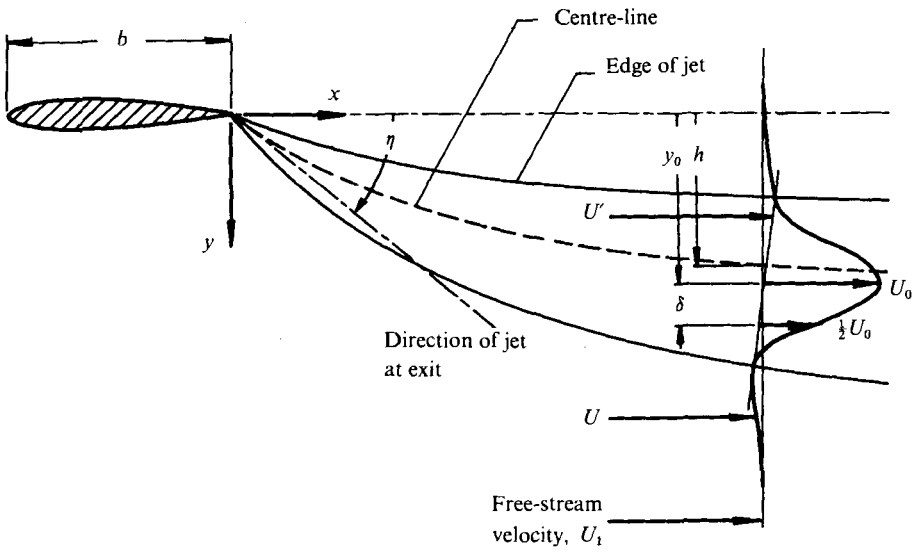

FIGURE 1. Schematic diagram of two-dimensional jet flap showing centre-line through centroids of velocity distributions between edges of the jet.

Unsteady jet flows attracted additional interest in aeronautics when W. R. Sears, according to Spence (1965), suggested the use of jet flaps for fast-acting lift control. A jet flap is obtained if air is ejected from a spanwise slot at or near the trailing edge of an aerofoil (figure 1). The lift control can be achieved by varying either the jet mass flow rate (pulsating jet) or the angle at which the jet emerges from the aerofoil (oscillating jet). These two types of unsteady jet appear to create distinctly different flow patterns. Lockwood (1963) first recognized the formation of ring vortices as a result of a pulsating axisymmetric jet flow and hypothesized a basic link between this vortex formation and the observed high secondary flow entrainment or thrust augmentation. Curtet & Girad (1973) confirmed the existence of these vortex patterns in their detailed flow-visualization studies of pulsating jets. Crow & Champagne (1971) were able to increase entrainment rates by using acoustic upstream stimulation to vary the nozzle exit velocity in an axisymmetric jet. This strong effect of jet pulsation on secondary flow entrainment was further established by Johnson & Yang (1968) and Bremhorst & Harch (1977). Much less information is available on a pulsating jet in a secondary stream. Williams, Ambrosiani & Palmer (1972) studied the effect of pulsating jet flow on the flow over an aerofoil flap at large flap angles. Chin (1977) recently made oscillatory surface pressure measurements over an aerofoil with a pulsating jet flap at the trailing edge.

The first measurements of the oscillatory jet flap characteristics were made by Trenka & Erickson (1970), Takeuchi (1970) and Simmons & Platzer (1971), and were followed by the experiments of Kretz (1973) and Simmons (1976*a*, *b*). These studies were all directed at the determination of the frequency response of lift on a jet-flapped aerofoil when either the jet exit angle is oscillated or the aerofoil is oscillated in pitch or plunge relative to the free stream. An experiment with an oscillating jet exhausting into still air was performed by Viets (1975), who used a rather unique and efficient fluidic nozzle for jet actuation.

Most of these unsteady jet studies relied on either flow visualization, measurement of the entrainment rate or measurement of the frequency response of the lift. Only the studies of pulsating jets by Bremhorst & Harch (1977) and Crow & Champagne (1971) provide detailed flow information. No similar study of oscillating jet flow seems to have been undertaken. Since the available oscillating jet flap theory, as will be shown in the next section, is incapable of predicting the frequency response of lift measurements on an aerofoil it appeared desirable to measure the oscillating jet characteristics directly and to deduce a viable theory from this information.

2. Oscillating jet flap theory

A complete solution of the steady jet flap problem on the basis of two-dimensional inviscid flow and thin-aerofoil theory was first given by Spence (1956). He assumed the jet to be separated along its boundaries from the external flow region by vortex sheets across which there is continuity of pressure but no flow. The use of the Bernoulli equation together with the irrotationality condition in both the jet flow and the external flow region then leads to the well-known condition that the pressure difference Δp across the jet is proportional to the jet momentum flux and inversely proportional to the radius of curvature r of the jet, i.e.

$$\Delta p = \rho U^2 d/r, \tag{1}$$

where ρ, U and d are the jet density, mean velocity and thickness respectively.

If in the limit the jet velocity goes to infinity while the jet momentum flux is kept constant, the jet thickness must become zero and the jet is represented by a single vortex distribution. On invoking the familiar approximations of thin-aerofoil theory, i.e. satisfaction of the flow tangency condition on the aerofoil chord line and on the x axis (figure 1) instead of along the actual jet position, the familiar integral equation for the downwash w and vortex distribution γ is obtained:

$$w(x) = -\frac{1}{2\pi}\int_{-b}^{\infty} \frac{\gamma(\xi)\,d\xi}{\xi - x}. \tag{2}$$

A more precise inspection shows that (2) represents a pair of simultaneous integro-differential equations. The boundary conditions are the prescribed jet slope at the aerofoil trailing edge and zero jet slope at downstream infinity. Spence was able to reduce this pair of equations to a single integro-differential equation and to construct a solution by Fourier-series approximation. It should be noted that the jet deflexion $h(x)$ logarithmically approaches infinity at downstream infinity in agreement with Woods's (1961, p. 397) statement on finite lift for semi-infinite configurations. In the meantime, the above jet model has been refined by satisfying flow tangency at the actual jet position and by incorporating jet entrainment effects (Halsey 1974).

The attempts to extend the thin-aerofoil concepts to the problem of a jet flap with an oscillating jet exit angle $\eta = \hat{\eta}\cos\omega t$ are due to Erickson (1962) and Spence (1965), who argued that the pressure difference across an oscillating jet can still be given by (1) if r is the local radius of curvature of the instantaneous jet centre-line. However, the solution of (2), where w and γ are now functions of time, presents enormous

difficulties. Spence (1965) proposed a 'weak jet' approximation by assuming the jet momentum coefficient C_j to be small with respect to four, where

$$C_j = (\text{momentum flux at nozzle per unit span})/(\tfrac{1}{2}\rho U_1{}^2 b). \tag{3}$$

He succeeded in deriving an approximation which is dependent only on the single parameter $\nu = \frac{1}{4}C_j k$ (where $k = \omega b/U_1$ is the reduced frequency). Spence found solutions to exist only for $\nu \leqslant 2$ and computed jet shapes and lift forces for both the oscillating jet case and the harmonically plunging jet-flapped aerofoil, while indicating only the basic approach for the harmonically pitching jet-flapped aerofoil. Trenka & Erickson (1970) completed Spence's solution for this last case and presented lift and pitching-moment results. They also drew attention to the 'boundary-layer' character of this approach due to the stretching transformation, which emphasizes the jet downstream of the trailing edge and which should lead to most accurate solutions at high reduced frequencies where the characteristic 'wavelength' $2\pi b/k$ is of order b or smaller.

The frequency-response measurements of Simmons & Platzer (1971), Kretz (1973) and Simmons (1976*b*) show trends which are directly opposite to Spence's predictions (e.g. see figures 8 and 9 in Simmons 1976*b*). On the other hand, the measurements by Takeuchi (1970) are in reasonable agreement with Spence's theory. A further disturbing aspect is noted by Spence (1965). His solution for the harmonically pitching jet-flapped aerofoil does not reduce to the classical pitching aerofoil theory for vanishingly small jet momentum coefficients. Also, it should be noted that Erickson (1962) and Spence (1965) prescribe the jet deflexion $h(x, t)$, slope and curvature to be zero infinitely far downstream. This requires that an oscillating jet, no matter how slow the oscillation might be, must return to zero jet deflexion at downstream infinity but must approach an infinite deflexion for the limiting case of vanishing frequency of oscillation. This point will be discussed further in §5.

More recently, Potter (1972) approached the oscillating jet flap problem as an initial-value problem in time and used point-vortex distributions to reduce (2) to finite-difference form. Initially, he specified the jet as a straight horizontal line, after which time the jet exit angle η was either changed instantaneously to a new constant value or continuously oscillated. With proper accounting for all the changes in bound and shed vorticity, in compliance with the conservation of total circulation for each time step, he was able to determine the jet shape by computing the downwash and the resultant velocities at each jet vortex point. Unfortunately, as is common with point-vortex methods, erratic vortex motions were found to build up with increasing time. This tended to limit the procedure to jet momentum coefficients C_j less than 0·1. As is shown in figures 8 and 9 of Simmons (1976*b*), Potter's computations agree substantially with the measurements of Simmons & Platzer (1971), Kretz (1973) and Simmons (1976*b*).

These conflicts among the theoretical and experimental results clearly show the need for the more thorough oscillating jet measurements which are described in the following sections.

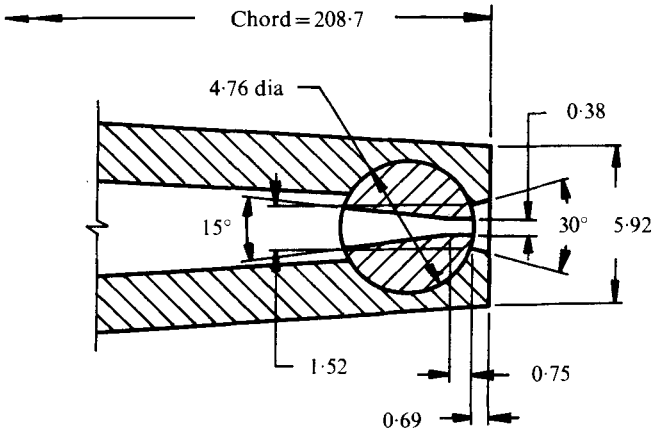

FIGURE 2. Cross-section of trailing edge of aerofoil showing rotatable nozzle. Dimensions in mm.

3. Experimental apparatus and procedure

3.1. *Wind tunnel and model*

The experiments were performed in the open-circuit wind tunnel in the Department of Mechanical Engineering, University of Queensland. The tunnel has a test section 1·22 m long with a 0·46 × 0·46 m square cross-section and corner fillets. Local mean velocities in the empty test section differed by not more than 0·4 % from the average test-section velocities used and r.m.s. turbulence levels were typically less than 0·1 %.

The model was a two-dimensional aerofoil with a 208·7 mm chord. It spanned the full 460 mm width of the test section in the horizontal plane midway between the top and bottom walls. The symmetric aerofoil section was generated from the NACA 0012 profile with a 228·6 mm chord by removing 8·7 % of the chord at the trailing edge to accommodate the nozzle for the jet flap. Details of the model, including the internal ducting of the air supply to produce an essentially two-dimensional jet, are described by Simmons (1976*b*). The nozzle, shown in cross-section in figure 2, comprised a converging duct leading into a slot with parallel sides spaced 0·38 mm apart. The slot extended along the full 460 mm span except for narrow spacers introduced every 50·8 mm to prevent excessive static and dynamic elastic distortion. Care was taken in the design of the trailing edge to avoid a Coanda effect on the emerging jet. Small amplitude oscillatory rotation of the nozzle was provided by a hydraulic actuator and a crank mechanism. Displacement feedback to the control valve of the actuator reduced drift and distortion in the sinusoidal nozzle rotation to an insignificant level.

3.2. *Instrumentation*

The jet-induced thrust on the model was measured with a balance in stationary air. The instantaneous angle of rotation of the nozzle η was measured with a variable-capacitance transducer attached to the crank. Instantaneous air velocities were obtained by traversing the probe of a hot-wire anemometer in the plane normal to the slot and at the mid-span of the aerofoil. A constant-temperature hot-wire anemometer with linear dynamic response and of local design and manufacture was used. Because of the unique bridge and control circuitry, both the stablity of the system

as measured by the damping ratio and the natural frequency of the anemometer at frequencies below 30 kHz are invariant with fluid velocity. The system also has absolute bridge balance at steady-state velocities, is independent of cable impedance, has transient free switching of the resistance ratio and has complete control over both the bandwidth and the damping ratio. Linearization of the wire current I in terms of the magnitude of the instantaneous wire cooling velocity vector **C** was achieved by implementation of the following equation with analog computer components:

$$I^2 = \alpha + \beta\sqrt{C} + \gamma C. \tag{4}$$

The constants α, β and γ were obtained by static calibration.

The hot wire was 10 μm diameter by 5 mm long platinum–iridium and was aligned parallel to the slot so that the instantaneous wire cooling velocity vector **C** was given by

$$\mathbf{C} = (U+u)\mathbf{i} + v\mathbf{j} \tag{5}$$

in terms of the mean and fluctuating components U and u in the x direction and the fluctuation v in the y direction (see figure 1); **i** and **j** being unit vectors in x and y directions.

In the small perturbation experiments in this investigation both u and v are small compared with U, so that time averaging C yields

$$\bar{C} = U. \tag{6}$$

Squaring and time averaging (5) yields

$$\overline{c^2} = \overline{u^2} + \overline{v^2}. \tag{7}$$

Here c is a small perturbation in C about the mean $\bar{C}$.

The velocities measured were too low to introduce compressibility effects except at the station closest to the slot, where the Mach number reached 0·5 in some tests. Interest at this station was restricted mainly to the location of the jet and so no correction for compressibility was made.

3.3. *Data analysis*

Data were stored on an FM tape recorder with a bandwidth of 1250 Hz and analysed subsequently on the EAI 600 hybrid computing system in the Faculty of Engineering at the University of Queensland. The use of the sinusoidal variation $\hat{\eta}\cos\omega t$ of the nozzle angle as a reference signal made it possible to study the velocity field at each of twelve sample times $t = \tau_i$ during one period $T = 2\pi/\omega$ of nozzle oscillation, where τ_i is given by

$$\tau_i = \tfrac{1}{12}(i-1)T, \quad i = 1, 2, \ldots, 12. \tag{8}$$

The positive-going zero crossings at the start and end of each period of the nozzle rotation signal were used to define the start and end of an ensemble in the linearized anemometer signal. About 300 successive ensembles were sampled at each τ_i and stored in a normalized histogram with 201 cells as an approximation to the velocity probability density distribution $p_c(\tau_i, x, y)$ at each x, y location of the hot wire. The histograms were then used in the calculation of the ensemble-mean velocity

$$\bar{C}(\tau_i, x, y) = E(C) \tag{9}$$

and the ensemble variance

$$\sigma^2(\tau_i, x, y) = E(C^2) - (E(C))^2, \tag{10}$$

Test number	U_1 (m/s)	C_j	θ (mm)	$\hat{\eta}$ (rad)	k	$\frac{U_j}{U_1}$	$R \times 10^{-5}$
1	29·2	0·098	10·2	0·0910	0·450	4·7	3·9
2	29·2	0·098	10·2	0·0910	0·900	4·7	3·9
3	29·2	0·098	10·2	0·0910	0·180	4·7	3·9
4	19·7	0·42	43·8	0·0910	0·946	9·4	2·7
5	19·7	0·42	43·8	0·0910	0·378	9·4	2·7
6	10·3	0·21	21·9	0·0650	3·18	6·8	1·4

TABLE 1

where E is the ensemble expectation operator. Statistics of the velocity field are thus obtained as a function of the nozzle angle η through the sample times τ_i. The ensemble-average velocity $\bar{C}(\tau_i, x, y)$ is not equal to the time-average velocity because of fluctuations due to the nozzle rotation which are superimposed on fluctuations due to the turbulent mixing process. If velocity fluctuations due to nozzle rotation are deterministic they will not contribute to the ensemble variance $\sigma^2(\tau_i, x, y)$. The ensemble variance is then a measure of the intensity of turbulence provided that the two velocity fluctuation processes are independent. Then

$$\sigma^2 = \overline{u^2} + \overline{v^2}. \tag{11}$$

This point is considered further in §4.2.

This data analysis scheme was run in real time on the hybrid computer. The histogram generation was overlapped with the analog-to-digital conversion. The digital section of the computer was used for overall control, generation of histograms, data storage on disc, post real time analysis and output. The analog section was used to linearize the anemometer output and to provide logic networks which used the nozzle angle to synchronize the sampling of ensembles.

3.4. *Experimental conditions*

Six tests were made under the conditions in table 1. The aerofoil was fixed at zero incidence to the free stream and the jet was oscillated through small angles about a mean direction parallel to the free stream. The jet momentum coefficient C_j and the jet momentum thickness $\theta = \frac{1}{2}bC_j$ were determined by assuming that the measured jet-induced thrust on the model was equal to the jet momentum flux at the nozzle exit. This is not strictly true because of pressure in the vicinity of the trailing edge caused by entrainment into the jet. The momentum flux at the nozzle exit is difficult to measure because of the narrow slot but it has been shown to exceed the jet-induced thrust by less than 6 % over the range of jet strengths and jet exit angles used in these tests (Korbacher & Sridhar 1960, p. 72). The jet velocity U_j at the nozzle exit was calculated from knowledge of the jet-induced thrust, nozzle width and jet exit plane pressure. Velocity profiles were measured up to 0·65 m (i.e. 3·16 chords or 1730 nozzle widths) downstream of the nozzle. The free-stream velocity was determined from hot-wire measurements outside the jet in the manner discussed in §4.1. The Reynolds numbers R in table 1 are based on the free-stream velocity and aerofoil chord.

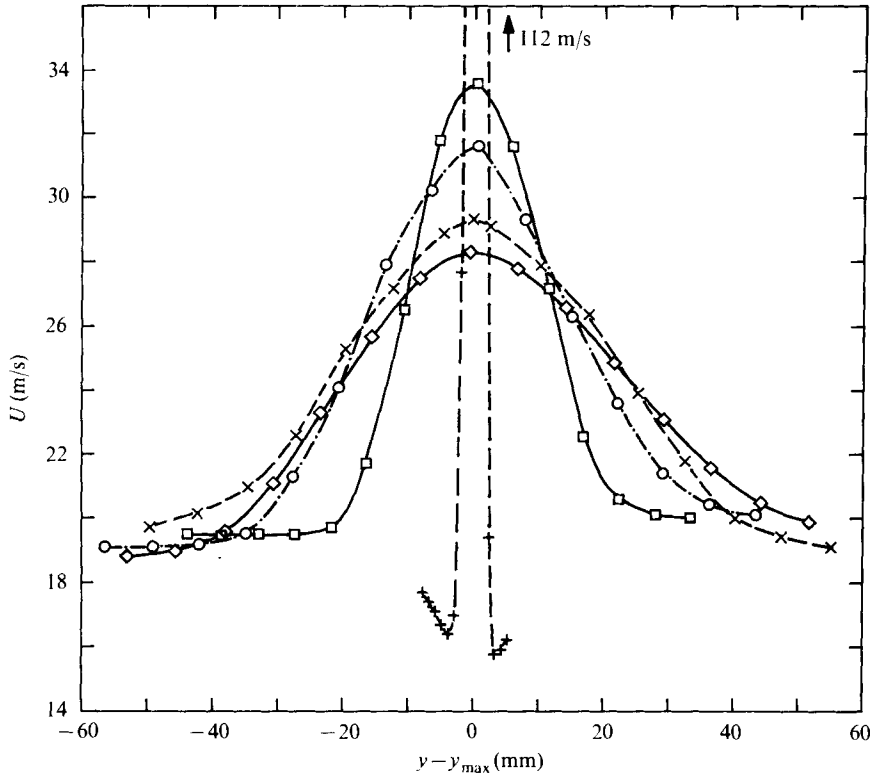

FIGURE 3. Some instantaneous velocity profiles for test 5 (U_1 = 19·7 m/s, U_j/U_1 = 9·4, k = 0·378). y_{max} is point of maximum velocity. +, x = 0·0132 m, τ/T = 0; □, 0·236 m, 0; ○, 0·458 m, 0; ◇, 0·658 m, 0; ×, 0·658 m, 0·5.

4. Experimental results and discussion

4.1. *Velocity profiles*

A small perturbation argument was used to obtain (6) and it follows similarly that the ensemble-average velocity $\tilde{C}(\tau_i, x, y)$ can be taken equal to $\tilde{U}(\tau_i, x, y)$. Its distribution over y for a given x and τ_i is called an 'instantaneous velocity profile' in this paper. The five instantaneous velocity profiles in figure 3 are representative of the 450 profiles measured and exhibit a number of the features of a steady jet flap. The slightly skewed profiles and the small velocity difference between the tails on opposite sides of each jet profile also occur in a steady jet flap (Dimmock 1955) as a consequence of its curvature. Hence velocity gradients in the y direction for both a steady jet flap and the instantaneous flow field of an unsteady jet flap are due to at least two causes. First, gradients within the jet are predominantly due to turbulent mixing, and second, much smaller gradients outside the jet are due to varying curvature of the path lines. Unsteady aerodynamic effects are likely to influence the jet velocity profile at sufficiently high frequencies of oscillation but further investigation is needed to clarify this aspect. The influence of the wake shed from the blunt trailing edge was measurable only at the station closest to the nozzle (viz. at x = 13·2 mm or 32·5 nozzle widths). This same station appears to be slightly downstream of the potential core.

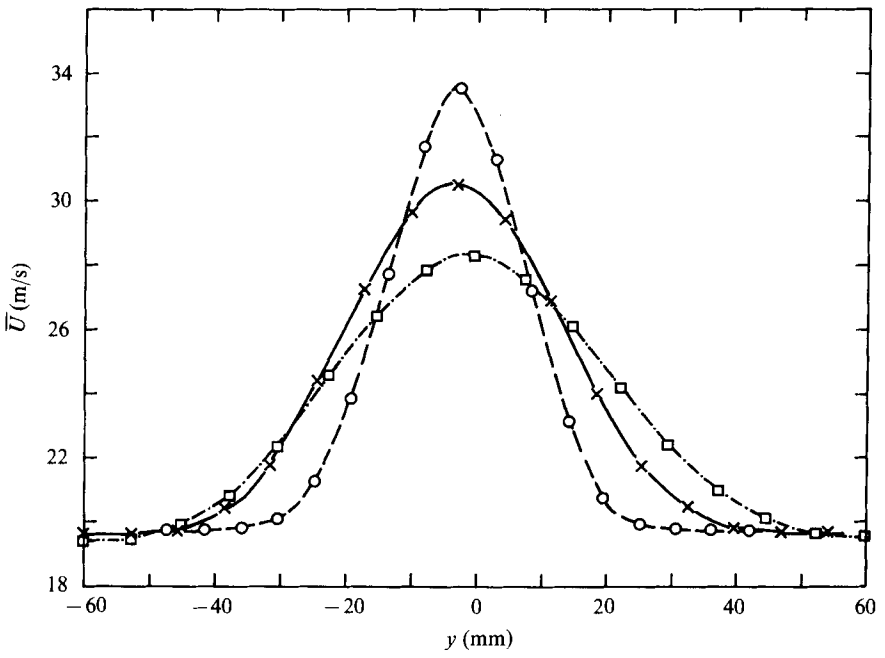

FIGURE 4. Mean velocity profiles for test 5 (U_1 = 19·7 m/s, U_j/U_1 = 9·4, k = 0·378) plotted with y = 0 at centre-line of wind tunnel. ○, x = 0·234 m; ×, x = 0·458 m; □, x = 0·658 m.

Mean velocity profiles, represented by those in figure 4, were obtained by averaging the instantaneous velocity profiles at a given x over all twelve sample times τ_i. Their symmetry and the approach of their tails to the same velocity (within experimental error) at different downstream stations indicate that periodically varying jet curvature causes velocities outside the jet to fluctuate symmetrically about a value very close to that of the free-stream velocity U_1. The values of U_1 in table 1 were obtained from measurements of the tails of the mean velocity profiles.

A similarity between the structures of an unsteady jet flap and a steady plane jet issuing into a parallel air stream is apparent when excess velocities are plotted. Excess velocity profiles are generated by subtracting from the instantaneous profiles a velocity distribution $U'(y)$ which varies linearly between the opposite edges of the jet y_1 and y_2:

$$U'(y) = \frac{[y-y_2][U(y_1)-U(y_2)]}{y_1-y_2} + U(y_2) \quad \text{for} \quad y_1 \geqslant y \geqslant y_2. \tag{12}$$

The instantaneous edges were found with reasonable accuracy at times and locations associated with a perceptible increase in the intensity of turbulence above its free-stream value. The shapes of the instantaneous excess velocity profiles in figures 5 and 6 have been normalized by the maximum excess velocity U_0 and by δ (the half-width or difference between the y co-ordinates at which the excess velocities are U_0 and $\frac{1}{2}U_0$). The shapes are similar over a range of flow conditions and for distances up to 1730 slot widths downstream of the nozzle. This self-preserving shape differs insignificantly from that measured by Bradbury & Riley (1967) for a steady plane jet issuing into a parallel air stream. Hence over the range of conditions of these tests, the instantaneous velocity profile in the oscillating jet can be quite accurately regarded

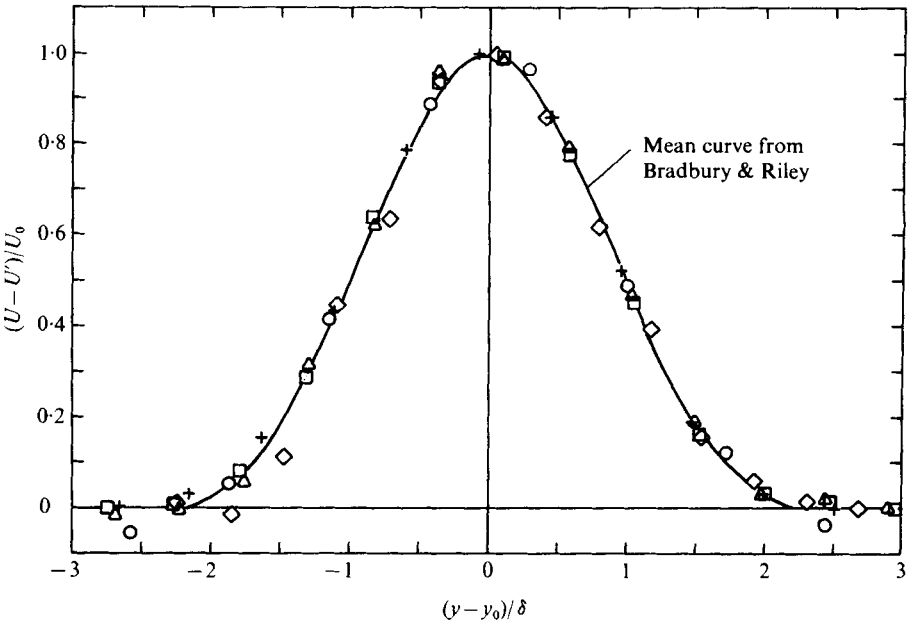

FIGURE 5. Some instantaneous excess velocity profiles for test 3 ($U_1 = 29{\cdot}2$ m/s, $U_j/U_1 = 3{\cdot}9$, $k = 0{\cdot}180$). ○, $x = 0{\cdot}0132$ m, $\tau/T = 0{\cdot}75$; □, 0·236 m, 0·75; +, 0·236 m, 0; △, 0·458 m, 0; ◇, 0·658 m, 0.

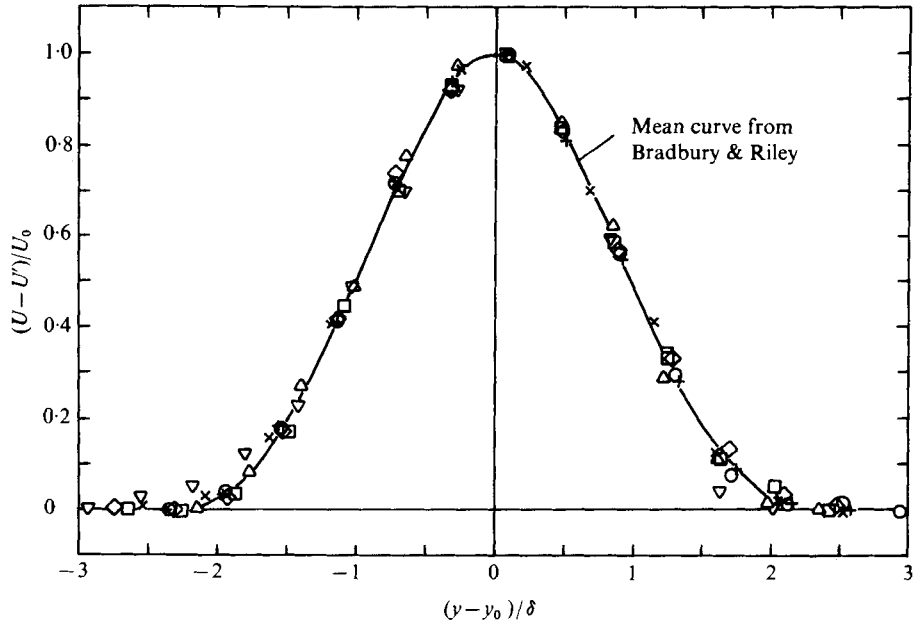

FIGURE 6. Some instantaneous excess velocity profiles for runs 1, 2, 4, 5 and 6. ○, test 1, $x = 0{\cdot}394$ m, $\tau/T = 0{\cdot}75$; □, test 2, 0·394 m, 0; +, test 4, 0·172 m, 0·75; △, test 4, 0·331 m, 0·75; ◇, test 5, 0·458 m, 0; ×, test 6, 0·267 m, 0; ▽, test 6, 0·658 m, 0·75.

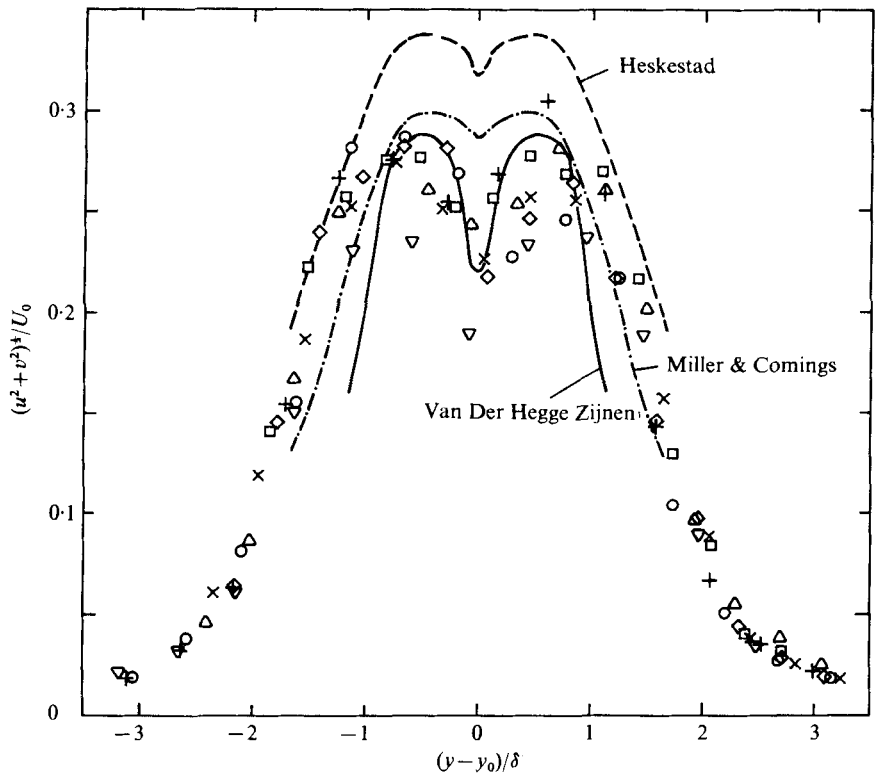

FIGURE 7. Turbulence intensity distributions and comparison with other measurements for $U_1 = 0$. △, test 2, $x = 0{\cdot}394$ m, $\tau/T = 0{\cdot}75$; ▽, test 3, 0·236 m, 0·75; ◇, test 4, 0·331 m, 0·75; ○, test 5, 0·236 m, 0·75; ×, test 5, 0·458 m, 0·75; □, test 5, 0·658 m, 0·75; +, test 6, 0·394 m, 0·75.

as the sum of the velocity profile across a steady jet parallel to the free stream and an approximately linear shear profile. The latter profile represents the velocity difference across the jet.

4.2. *Turbulence measurements*

Two random processes can contribute to the measured ensemble variances $\sigma^2(\tau_i, x, y)$, namely fluctuations due to turbulent mixing within the jet and fluctuations in the relative location of the hot wire and the instantaneous velocity profile when the velocity is sampled. The first process does not introduce bias into the estimate of $\tilde{U}(\tau_i, x, y)$. The second process could conceivably result from randomness in the nozzle rotation or the sampling time, or from large-scale random fluctuations in the flow. If significant, it would bias $\tilde{U}(\tau_i, x, y)$ to an extent dependent on y. This would result from the nonlinear relationship between the location of the hot wire relative to the instantaneous velocity profile and the velocity at the hot wire.

Some measured distributions of ensemble variance over a range of test conditions are plotted in figure 7 under the assumption that they are due entirely to the intensity of turbulent mixing [i.e. $\sigma^2(\tau_i, x, y)$ is equated to $\overline{u^2}+\overline{v^2}$ as a consequence of (11)]. The assumption appears reasonable because of the similarity of the distributions for different conditions when based on the length scale δ. A more quantitative justi-

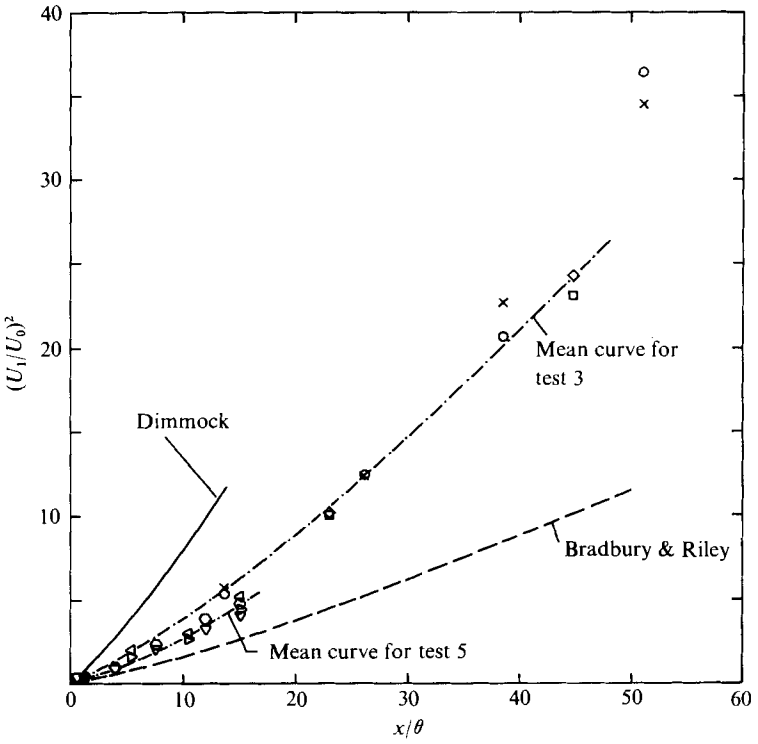

FIGURE 8. Decay of maximum of instantaneous excess velocity profile for various conditions. Steady measurements from Bradbury & Riley (1967) are plotted with effective origin at $x = 0$. Steady measurements from Dimmock (1955) are for $\eta = 0{\cdot}548$ rad and $C_f = 0{\cdot}3$. Mean curves for tests 3 and 5 are averages over all sampling times τ_i and are used in §5. ○, test 2, $\tau/T = 0{\cdot}75$; ×, test 2, 0; □, test 3, 0·75; ◇, test 3, 0; ▽, test 4, 0·75; ⬡, test 4, 0; test ▷, test 5, 0·75; ◁, test 5, 0.

fication is the similarity to the measurements of Heskestad (1965), Van Der Hegge Zijnen (1958) and Miller & Comings (1957) for a steady two-dimensional jet with zero secondary flow (i.e. $U_1 = 0$). However, it should be noted that these investigators measured closer to the nozzle (in terms of nozzle widths). Turbulence intensity measurements in a two-dimensional steady jet with secondary flow are scarce but those by Bradbury & Riley (1967), which are limited to the jet centre-line, indicate that $\overline{u^2}$ is not very sensitive to values of U_1/U_0 from zero to those generated in the present test. The slow decrease of $\overline{u^2}$ with decreasing U_1/U_0 measured by Bradbury & Riley is consistent with the decrease in $\overline{u^2}+\overline{v^2}$ measured in these tests as the measuring station approaches the nozzle. It should be restated here that the velocity fluctuations were band-limited to 1250 Hz by the tape recorder.

The structure of turbulence in an oscillating jet is of interest in entrainment studies but it was not a major part of this investigation. Aspects such as self-preservation and stationarity need further study. Sufficient results are presented here to identify turbulence as the main cause of variance in measurements and to indicate a further similarity between the structure of steady and oscillating jets.

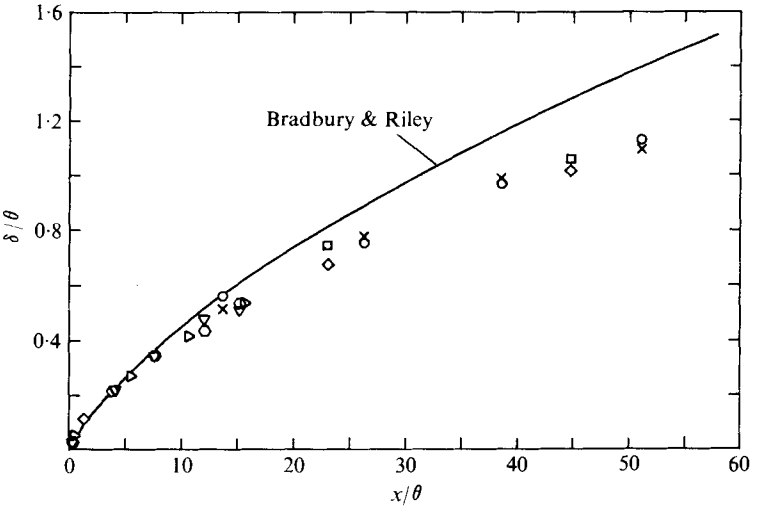

FIGURE 9. Spread of instantaneous excess velocity profile for various conditions. Steady measurements from Bradbury & Riley (1967) are plotted with effective origin at $x = 0$. ○, test 2, $\tau/T = 0{\cdot}75$; ×, test 2, 0; □, test 3, 0·75; ◇, test 3, 0; ▽, test 4, 0·75; ⬡, test 4, 0; ▷, test 5, 0·75.

4.3. *Measurements of jet decay and spread*

Representative measurements of the decay and the spread of the instantaneous velocity profile are plotted in figures 8 and 9. Dimensional analysis of a steady plane jet in a parallel secondary flow (Bradbury & Riley 1967) yields the jet momentum thickness $\theta = \frac{1}{2}bC_j$ as the appropriate length scale in the free-stream direction for fully turbulent regions far enough downstream to be independent of precise nozzle conditions (such as the slot width, jet exit velocity and trailing-edge geometry). The same length scale is used here for the unsteady jet to enable a comparison with steady measurements. In figures 8 and 9 the range of x is 370–1730 nozzle widths. The distance downstream at which rates of jet decay and spread become independent of precise nozzle conditions is known to depend on those nozzle conditions. However, the shift of the so-called 'effective origin' from the nozzle is small in these tests compared with the range of x.

The measurements by Bradbury & Riley (in figures 8 and 9) have been averaged over a range of flow conditions and have been corrected for shifts of the effective origin from the nozzle exit, i.e. they are plotted with shifts assumed to be zero. It is apparent that the rate of jet decay is influenced by the jet exit angle η. The measured rates of decay of the oscillating jet are physically consistent in that they lie between the steady measurements by Bradbury & Riley at zero η and the steady measurements by Dimmock (1955) at large η. It should also be noted that the more rapid decays among the oscillatory jet measurements are associated with jets having higher values of the product kC_j. Near the trailing edge the rates of spreading of the oscillating jet are similar to those measured by Bradbury & Riley but become smaller further downstream. The shear processes in a curved jet are not well understood and remain a subject for further investigation.

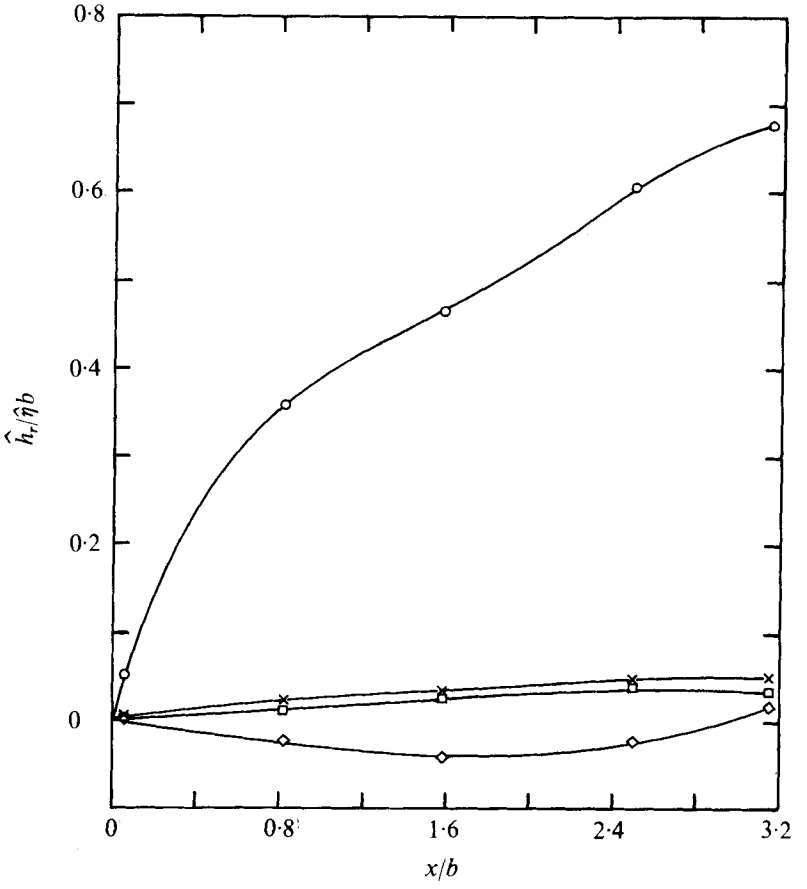

FIGURE 10. Measured Fourier components h_r of displacement of jet centre-line for test 4. ◇, $r = 0$ (mean), ○, $r = 1$ (fundamental); □, $r = 2$ (second harmonic); ×, $r = 3$ (third harmonic).

4.4. *Measurements of instantaneous jet position*

The jet centre-line is defined in this study as the locus of centroids of the instantaneous velocity profiles at a given τ_i. Use of the line of maximum jet velocity is regarded as less appropriate in view of the skewness in the velocity profiles. At a given x the ensemble-average transverse deflexion h of the jet centre-line is a function of time with period $2\pi/\omega$ and was measured at each of twelve sample times τ_i. This function was decomposed by Fourier analysis into its mean and its fundamental, second and third harmonics. The amplitudes of these four components for test 4 are plotted in figure 10 to illustrate the dominance of the fundamental for about three chord lengths downstream. The chord is introduced as the length scale at this point because interest is now centred on the gross movement of the jet flap relative to the aerofoil rather than on the internal structure of the jet. For the other tests measurements of the relative magnitudes of the four Fourier components were similar to those in figure 10.

The fundamental component of $\tilde{h}(t, x)$ can be written as $\hat{h}(x)\cos(\omega t + \phi(x))$, where ϕ is the phase angle relative to the nozzle oscillation. Figures 11–13 are graphs of the measured $\hat{h}(x)$ and $\phi(x)$ for various jet momentum coefficients and frequencies

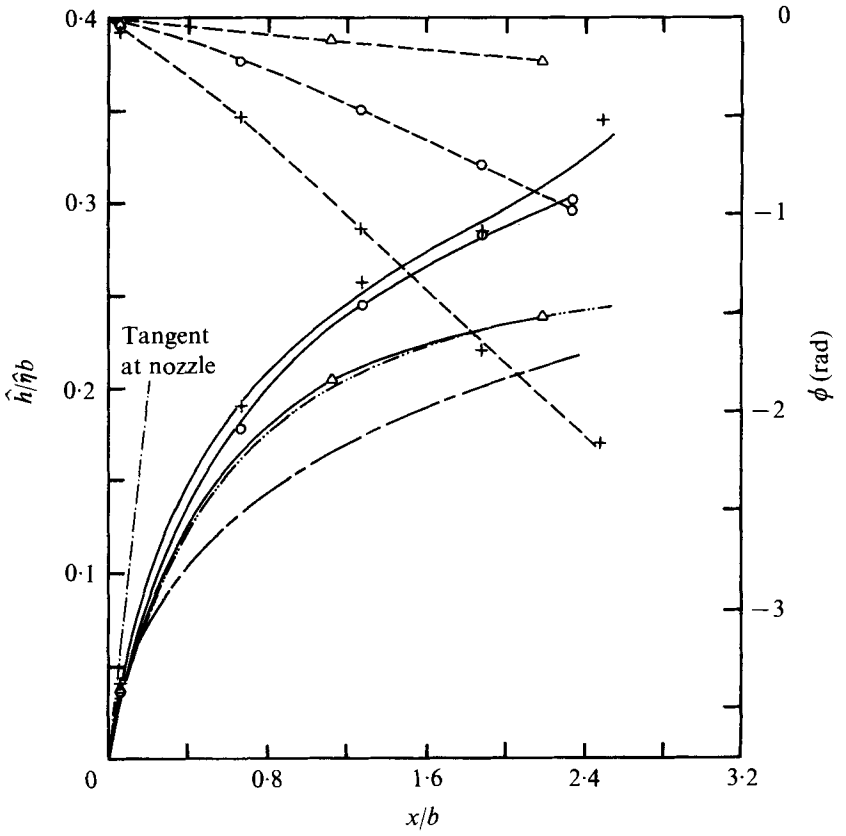

FIGURE 11. Measured amplitude and phase of fundamental component of displacement of jet centre-line for $C_j = 0{\cdot}098$ and three frequencies. △, test 3, $k = 0{\cdot}180$; ○, test 1, $k = 0{\cdot}450$; +, test 2, $k = 0{\cdot}900$; ——, amplitude; – – –, phase; — – —, steady theory of Spence ($C_j = 0{\cdot}1$); — · · —, steady measurements of Dimmock ($\eta = 0{\cdot}548$ rad, $C_j = 0{\cdot}1$).

of nozzle oscillation. Also included are two steady jet centre-lines, one predicted by the theory of Spence (1956) and the other obtained by interpolation between measurements made by Dimmock (1955). The envelopes of transverse oscillation of the centre-line (defined by $\hat{h}(x)$) and the centre-line for the steady jet flap are similar, especially at the lower frequencies of nozzle oscillation. An increase in frequency in general causes $\hat{h}(x)$ to increase, a striking example being the measurements in figure 13 for the test at a relatively high frequency. Note that the waviness in curves for $\hat{h}(x)$ at the higher frequencies cannot be attributed to experimental error.

The instantaneous jet centre-lines in figures 14 and 15 have been constructed from the measurements of $\hat{h}(x)$ and $\phi(x)$. A marked disagreement with the predictions of Spence (1965) is shown in figure 15. The measurements indicate that particles on the jet centre-line move along paths which diverge from the line $y = 0$, whereas Spence predicts particle paths which approach $y = 0$ as x increases.

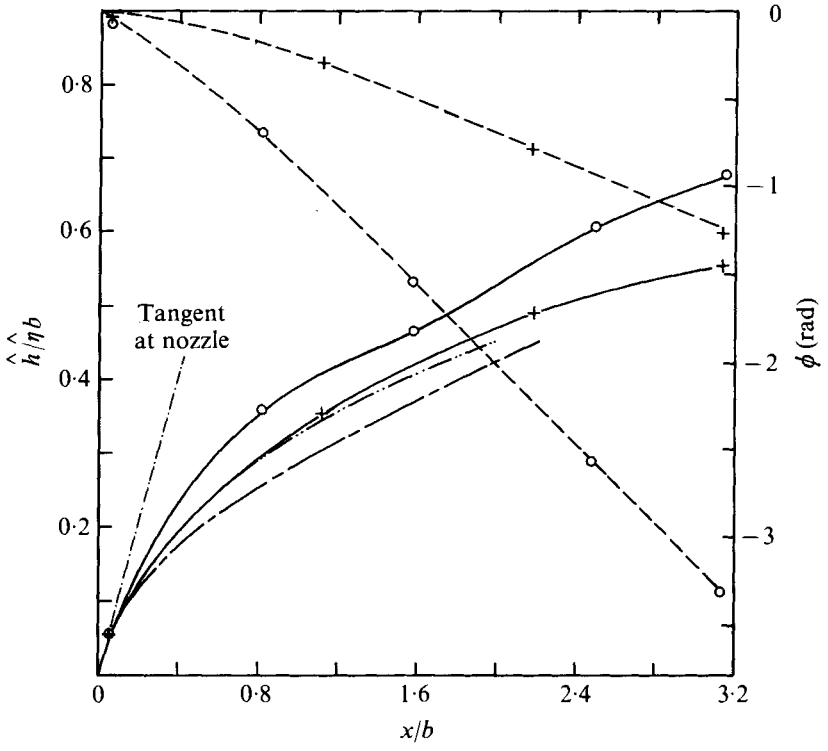

FIGURE 12. Measured amplitude and phase of fundamental component of displacement of jet centre-line for $C_j = 0{\cdot}42$ and two frequencies. +, test 5, $k = 0{\cdot}378$; ○, test 4, $k = 0{\cdot}946$; ——, amplitude; - - - -, phase; — — —, steady theory of Spence ($C_j = 0{\cdot}42$); — · · —, steady measurements of Dimmock ($\eta = 0{\cdot}548$ rad, $C_j = 0{\cdot}42$).

5. A quasi-steady jet flap model

In view of the considerable complexity of the available oscillatory jet flap theories it appears to be meaningful to explore the usefulness of a quasi-steady model in which the oscillatory flow is considered as a succession of steady flows. Thus, by using thin-aerofoil concepts, the jet is idealized by an infinitely thin vortex sheet divided into vortex elements. Each element is assumed to travel along that particular steady jet path which corresponds to the jet exit angle at the time of ejection of the element from the trailing edge. The velocity of travel of the elements is found from the available measured jet decay data. This model is shown schematically in figure 16, where the jet exit angle is given by

$$\eta = \mathrm{Re}[\hat{\eta}\exp(ikU_1 t/b)] \tag{13}$$

(Re denotes the real part of the complex quantity). This procedure enables the separate determination of the components of the flow field in phase and in quadrature with η. For example, the lift L on the aerofoil is expressed in terms of in-phase and quadrature components L_R and L_I by

$$L = \mathrm{Re}[(L_R + iL_I)\exp(ikU_1 t/b)]. \tag{14}$$

Only L_R is generated by the flow at the instant when $t = 0$ (corresponding to the maximum downward jet exit angle). Similarly only L_I is generated at the instant

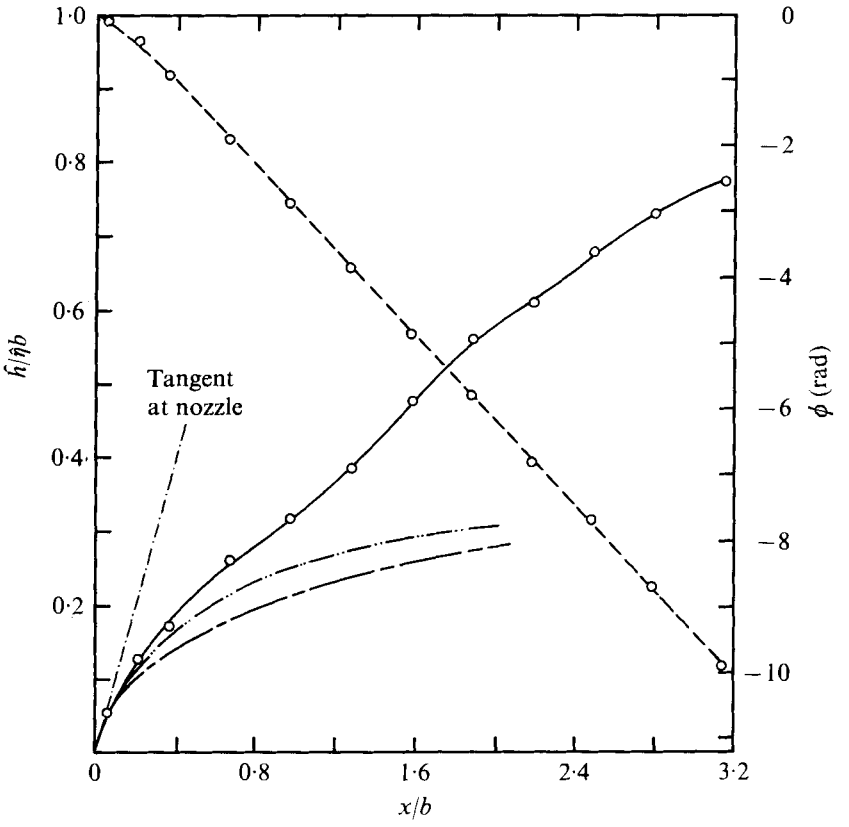

FIGURE 13. Measured amplitude and phase of fundamental component of displacement of jet centre-line for test 6 (C_j = 0·21, k = 3·18). ——, amplitude; – – – –, phase; — — —, steady theory of Spence (C_j = 0·21); — · · —, steady measurements of Dimmock (η = 0·548 rad, C_j = 0·21).

when $kU_1t/b = \frac{3}{2}\pi$ (corresponding to zero jet exit angle during the downward stroke).

This quasi-steady model leads to the instantaneous jet centre-lines in figure 14 for reduced frequencies k corresponding to the lowest two values used in the experiments. The steady jet path used is that computed by Spence (1956). The velocity of the vortex element at a given x is obtained by averaging the maxima of the measured instantaneous velocity profiles over a cycle of oscillation. The decay of this velocity with x is plotted in figure 8. These instantaneous jet centre-lines are in reasonable agreement with the measured jet centre-lines, allowing for the fact that the steady theory of Spence underestimates the steady jet deflexion (see figures 11 and 12 in this paper and figure 6 in Spence 1956).

Further support for the applicability of quasi-steady concepts at low frequencies can be found from the close similarity between the oscillating and steady jet characteristics as evidenced by the time-averaged velocity profiles (figure 4), the instantaneous excess velocity profiles (figures 5 and 6), the turbulence intensity (figure 7) and the jet decay and spreading (figures 8 and 9). The previously noted difference in downstream conditions in Spence's two models (namely zero jet deflexion for the oscillating jet and a logarithmically infinite deflexion for the steady jet) is naturally resolved by

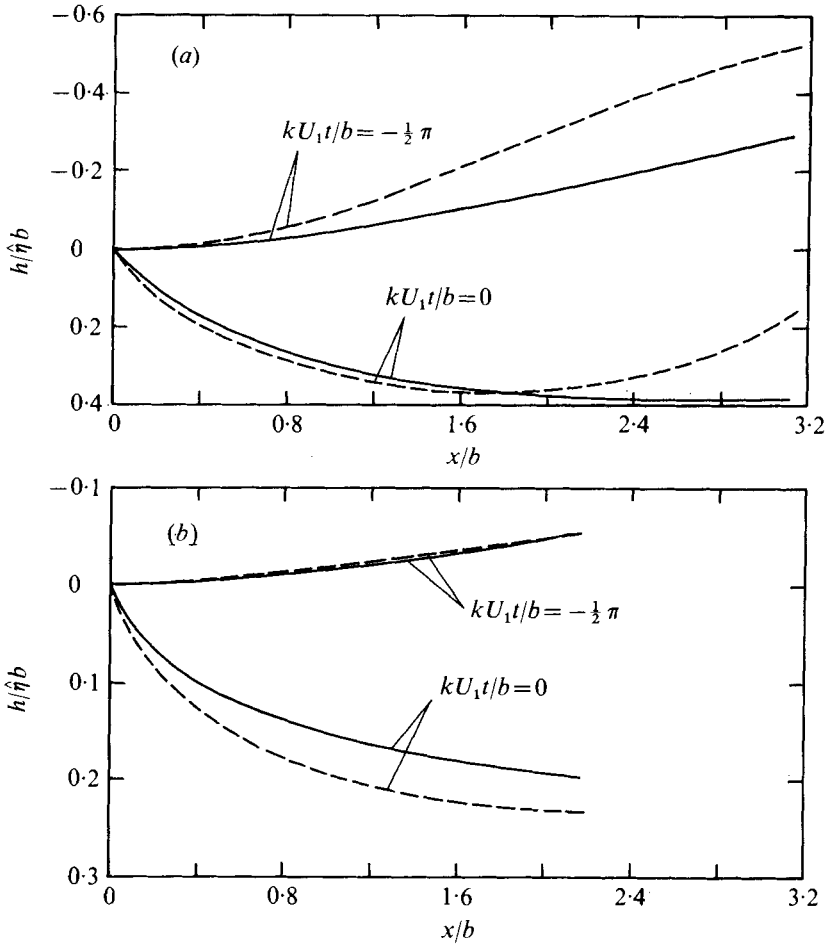

FIGURE 14. Jet centre-lines at two instants. (*a*) Test 5. (*b*) Test 3. – – –, measured; ——, model (using decay of maximum jet velocity).

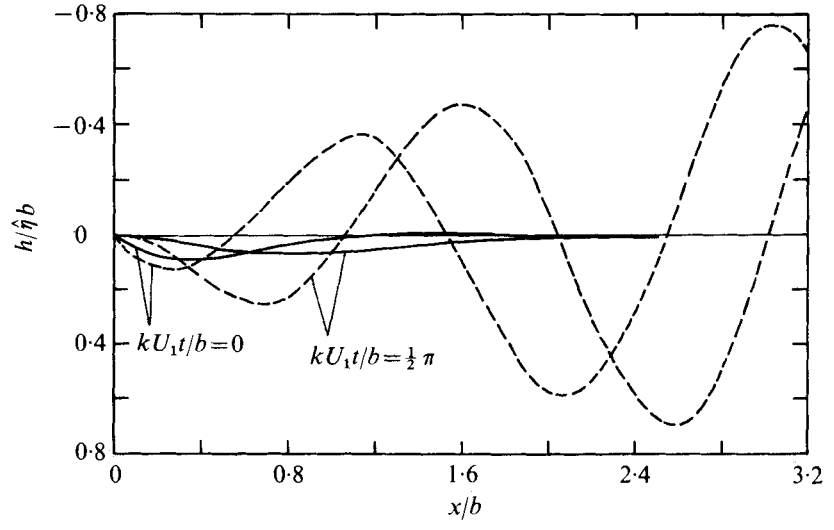

FIGURE 15. Comparison of instantaneous jet centre-lines for test 6 ($C_j = 0{\cdot}21$, $k = 3{\cdot}18$) with oscillatory theory of Spence ($C_j = 0{\cdot}25$, $k = 3{\cdot}2$). – – –, measured; ——, Spence.

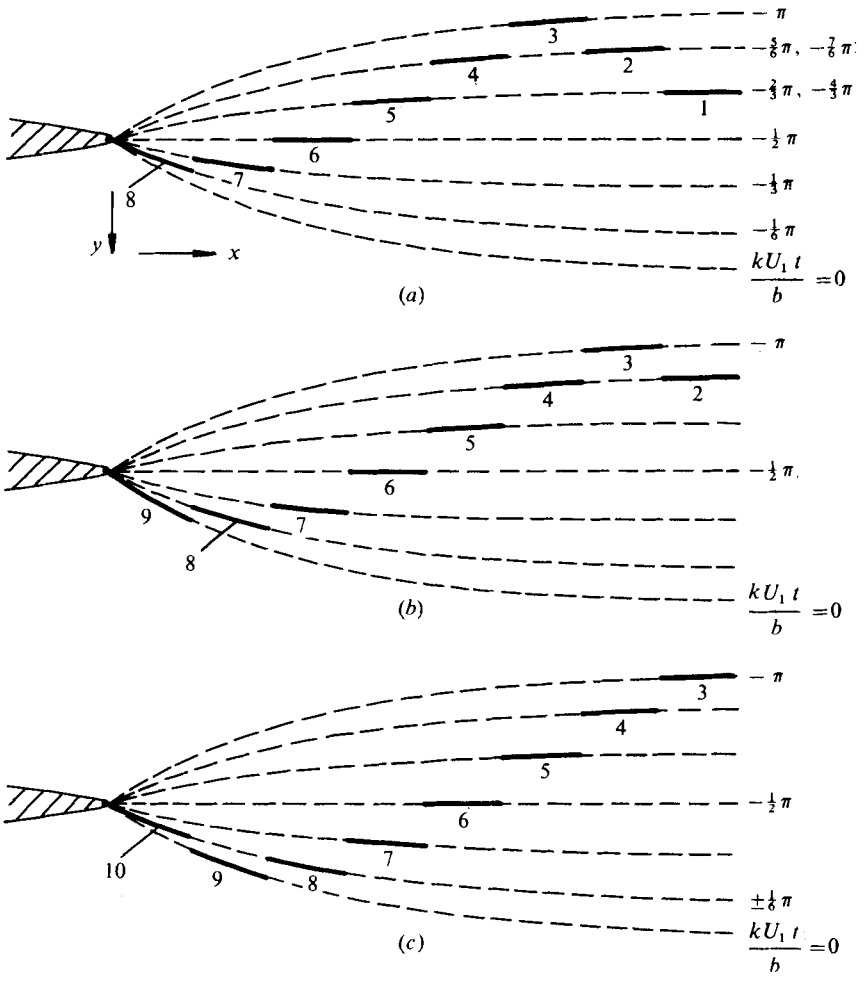

FIGURE 16. Schematic diagram of position of vortex elements (solid lines) along steady jet paths (dashed lines) at three successive instants. (*a*) $kU_1t/b = \frac{1}{6}\pi$, (*b*) $kU_1t/b = 0$, (c) $kU_1t/b = +\frac{1}{6}\pi$. Times on paths are those at which elements left nozzle.

incorporating the velocity decay characteristics into the quasi-steady model. Hence sufficiently far downstream the jet velocity approaches the free-stream velocity, thus obviating the need for arguments previously advanced by Erickson (1962) and Spence (1965). For practical computational purposes it is well known that only the region of the jet within a few chord lengths of the trailing edge need be taken into account for accurate prediction of the lift and moment on the aerofoil. Use of Spence's steady thin-jet model, but with enforcement of the time-dependent flow tangency condition between the outer flow and the jet flow, results in a quasi-steady theory which predicts substantial phase lags for the frequency response of the lift. More detailed results will be reported in a future paper.

6. Conclusions

The hot-wire anemometer measurements of oscillating two-dimensional jets ejected from an aerofoil embedded in uniform low speed flow provide detailed information on the jet shape, velocity decay and spread as functions of the jet momentum coefficient and frequency of oscillation. The measured instantaneous velocity profiles and turbulence intensities indicate a close similarity between the structure of oscillating jets and steady jets. Comparison of jet spread and jet decay characteristics in a secondary flow show that oscillating jets decay more rapidly and spread less rapidly than steady jets parallel to the secondary flow. These measurements, together with those of the instantaneous jet centre-lines, suggest the applicability of a quasi-steady jet flap theory over a fairly wide range of frequencies. Unlike the unsteady theory of Spence, the proposed quasi-steady theory shows trends with increasing frequency which are compatible with the jet centre-lines measured at relatively high frequencies. Further measurements are needed to establish more thoroughly its range of validity.

The work described in this paper was supported by the Australian Research Grants Committee under Reference No. F70/17452 and by the US Naval Air Systems Command under Project No. WR-T-1581. The authors gratefully acknowledge the encouragement and support by Prof. K. J. Bullock (University of Queensland), Prof. R. W. Bell (Naval Postgraduate School) and Dr H. J. Mueller (Naval Air Systems Command) while the first and second authors were on leave at the Naval Postgraduate School and University of Queensland, respectively.

REFERENCES

Berner, F. & Hermann, M. 1972 *8th Int. Cong. Aero. Sci. A.I.A.A.*, 72–47.

Bradbury, L. J. S. & Riley, J. 1967 *J. Fluid Mech.* **27**, 381.

Bremhorst, K. & Harch, W. H. 1977 *A.S.M.E. Symp. Turbulent Shear Flows, Pennsylvania State Univ.*

Chin, Y. T. 1977 *Lockheed-Georgia Co. Rep.*

Crow, S. C. & Champagne, F. H. 1971 *J. Fluid Mech.* **48**, 547.

Curtet, R. M. & Girad, J. P. 1973 *A.S.M.E. Symp. Fluid Mech. Mixing.*

Dimmock, N. A. 1955 *Nat. Gas Turbine Establ. Rep.* R 175.

Erickson, J. C. 1962 Ph.D. thesis, Cornell University.

Foa, J. V. 1958 *Appl. Mech. Rev.* **11**, 655.

Halsey, N. D. 1974 *J. Aircraft* **11**, 540.

Harsha, P. T. 1971 *Arnold Enging Development Center Rep.* AEDC-TR-71-36.

Heskestad, G. 1965 *J. Appl. Mech.* **32**, 721.

Johnson, W. S. & Yang, T. 1968 *A.S.M.E. Winter Ann. Meeting Energy Systems Exposition.*

Korbacher, G. K. & Sridhar, K. 1960 *Inst. Aerophys., Univ. Toronto Rev.* UTIA 14.

Kretz, M. 1973 *Giravions Dorand, Suresnes, France Rep.* DE 07-44 E5.

Lockwood, R. M. 1963 *Hiller Aircraft Co. Rep.* ARD-308.

Miller, D. R. & Comings, E. W. 1957 *J. Fluid Mech.* **3**, 1.

Potter, G. E. 1972 Ph.D. thesis, Pennsylvania State University.

Simmons, J. M. 1976*a* *A.I.A.A. J.* **14**, 741.

Simmons, J. M. 1976*b* *A.I.A.A. J.* **14**, 1297.

SIMMONS, J. M. & PLATZER, M. F. 1971 *J. Aircraft* **8**, 587.

SPENCE, D. A. 1956 *Proc. Roy. Soc.* A **238**, 46.

SPENCE, D. A. 1965 *Phil. Trans. Roy. Soc.* A **257**, 445.

TAKEUCHI, K. 1970 M.S. thesis, Pennsylvania State University.

TRENKA, A. R. & ERICKSON, J. C. 1970 *Cornell Aero. Lab. Rep.* CAL AC-2260-S-1.

VAN DER HEGGE ZIJNEN, B. G. 1958 *Appl. Sci. Rev.* A **7**, 293.

VIETS, H. 1975 *A.I.A.A. J.* **13**, 1375.

WILLIAMS, J. R., AMBROSIANI, J. P. & PALMER, W. E. 1972 *Columbus Aircraft Div./North American Rockwell Rep.* NR 72H-325.

WOODS, L. C. 1961 *The Theory of Subsonic Plane Flow*. Cambridge University Press.